SIAM J. SCI. COMPUT.
Vol. 42, No. 4, pp. A2514–A2536

A HIGHLY EFFICIENT AND ACCURATE NEW SCALAR AUXILIARY VARIABLE APPROACH FOR GRADIENT FLOWS*

FUKENG HUANG†, JIE SHEN†, AND ZHIGUO YANG†

Abstract. We present several essential improvements to the powerful scalar auxiliary variable (SAV) approach. Firstly, by using the introduced scalar variable to control both the nonlinear and the explicit linear terms, we are able to reduce the number of linear equations with constant coefficients to be solved at each time step from two to one, so the computational cost of the new SAV approach is essentially half of the original SAV approach while keeping all its other advantages. This technique is also extended to the multiple SAV approach. Secondly, instead of discretizing the dynamical equation for the auxiliary variable, we use a first-order approximation of the energy balance equation, which allows us to construct high-order unconditionally energy-stable SAV schemes with uniform and, more importantly, variable time step sizes, enabling us to construct, for the first time, high-order unconditionally stable adaptive time-stepping backward differentiation formula schemes. Representative numerical examples are provided to demonstrate the improved efficiency and accuracy of the proposed method.

Key words. gradient flow, SAV approach, adaptive time-stepping, high-order methods, stability

AMS subject classifications. 65N35, 65N22, 65F05, 35J05

DOI. 10.1137/19M1298627

1. Introduction.

Dissipative physical systems are ubiquitous in the real world, due to the second law of thermodynamics. It is highly desirable for numerical methods targeted on such systems to preserve the discrete energy dissipation law. As such, many efforts to develop energy-stable numerical methods have been devoted to this longstanding and active research area. These include, but are not limited to, the average vector field method [8, 22], the convex splitting method [4, 5, 12, 13], the stabilization method [26, 33], the Lagrange multiplier method [14], and more recently, the invariant energy quadratization method [27, 32, 15] and the scalar auxiliary variable (SAV) method [23, 24, 16]. Among them, the SAV method is a particular powerful tool for the design of unconditionally energy-stable first- and second-order schemes for a large class of gradient flows. The aim of this paper is to present some essential improvements on the highly efficient SAV approach.

In order to motivate our improvements, we briefly review below the SAV approach for the general form of gradient flows:

$$\frac{\partial \phi}{\partial t} = -\mathcal{G}\mu, \tag{1.1}$$

where ϕ is the unknown function, $\mathcal{G}$ is a positive operator that gives rise to the dissipative mechanism of the system, e.g., $\mathcal{G} = \mathcal{I}$ in the L^2 gradient flow and $\mathcal{G} = -\nabla^2$ in the H^{-1} gradient flow, and μ is the so-called chemical potential

$$\mu = \frac{\delta E_{tot}}{\delta \phi} = \mathcal{L}\phi + U(\phi) \tag{1.2}$$

*Submitted to the journal's Methods and Algorithms for Scientific Computing section November 11, 2019; accepted for publication (in revised form) July 6, 2020; published electronically August 27, 2020.

https://doi.org/10.1137/19M1298627

Funding: The work of the second author was partially supported by NSF through grant DMS-2012585 and by AFOSR through grant FA9550-20-1-0309.

†Department of Mathematics, Purdue University, West Lafayette, IN 47907 (huang972@purdue.edu, shen7@purdue.edu, yang1508@purdue.edu).

with respect to the free energy

$$E_{tot}(\phi) = \frac{1}{2}(\phi, \mathcal{L}\phi) + E_1(\phi), \tag{1.3}$$

where $\mathcal{L}$ is a nonnegative linear operator and $E_1(\phi)$ is a nonlinear functional. For the sake of conciseness, homogeneous Neumann or periodic boundary conditions are assumed throughout the paper such that all boundary terms will vanish when integration by parts is performed.

The key for the SAV approach is to introduce a scalar variable $r(t)$ defined by $r(t) = \sqrt{E_1[\phi] + C_0}$ (C_0 is chosen such that $E_1[\phi] + C_0 > 0$) and its associated dynamical equation

$$\frac{dr}{dt} = \frac{1}{2\sqrt{E_1[\phi] + C_0}} \int_\Omega U[\phi] \frac{\partial \phi}{\partial t} d\Omega, \quad U[\phi] = \frac{\delta E_1}{\delta \phi}. \tag{1.4}$$

Then, a first-order SAV scheme with explicit treatment for all nonlinear terms is as follows:

$$\frac{\phi^{n+1} - \phi^n}{\Delta t} = -\mathcal{G}\mu^{n+1}, \tag{1.5a}$$

$$\mu^{n+1} = \mathcal{L}\phi^{n+1} + \frac{r^{n+1}}{\sqrt{E_1[\phi^n] + C_0}} U(\phi^n), \tag{1.5b}$$

$$\frac{r^{n+1} - r^n}{\Delta t} = \frac{1}{2\sqrt{E_1[\phi^n] + C_0}} \int U(\phi^n) \frac{\phi^{n+1} - \phi^n}{\Delta t} d\Omega. \tag{1.5c}$$

One can eliminate μ^{n+1} and r^{n+1} from the above coupled linear scheme to obtain a linear equation for ϕ only:

$$(I + \Delta t \mathcal{G}\mathcal{L})\phi^{n+1} = \phi^n - r^{n+1} \Delta t \mathcal{G} \left(\frac{U[\phi^n]}{\sqrt{E_1[\phi^n] + C_0}} \right). \tag{1.6}$$

Setting $\phi^{n+1} = \phi_1^{n+1} + r^{n+1}\phi_2^{n+1}$, we find that ϕ_1^{n+1} and ϕ_2^{n+1} are solutions of the following two linear equations with constant coefficients:

$$(I + \Delta t \mathcal{G}\mathcal{L})\phi_1^{n+1} = \phi^n, \quad (I + \Delta t \mathcal{G}\mathcal{L})\phi_2^{n+1} = -\Delta t \mathcal{G} \left(\frac{U[\phi^n]}{\sqrt{E_1[\phi^n] + C_0}} \right). \tag{1.7}$$

Once ϕ_1^{n+1} and ϕ_2^{n+1} are known, we can determine r^{n+1} explicitly from (1.5c) (see more details in [23, 24, 30]).

The above SAV approach enjoys the following remarkable properties:

- it requires only the solution of two linear systems with constant coefficients at each time step (efficiency);
- the first- and second-order SAV schemes are unconditionally energy stable (stability);
- it only requires the nonlinear energy functional $E_1(\phi)$ be bounded from below, so it is applicable to a large class of gradient flows (flexibility).

Our aim in this paper is to propose some new essential improvements on the SAV approach to make it even more efficient and flexible in the sense that

- it only requires solving one linear system with constant coefficients at each time step;

- it does not require the nonlinear energy functional $E_1(\phi)$ be bounded from below and is applicable to more general gradient flows, even to general dissipative systems;
- and more importantly, it is extendable to higher-order backward differentiation formula (BDF) type schemes with unconditional stability and amenable to higher-order adaptive time-stepping.

The rest of the paper is organized as follows. In section 2, we describe the construction of the new SAV scheme for gradient flows in a general form. In section 3, we construct the higher-order unconditionally energy-stable scheme. In section 4, adaptive time-stepping strategy for our unconditionally energy-stable schemes will be studied. In section 5, we provide ample numerical examples to demonstrate the performance of our proposed method, and comparisons with the original SAV method will be reported. Section 6 concludes the discussions with some closing remarks.

2. A new SAV energy-stable scheme. The SAV approach requires solving two linear equations at each time step. However, we observe that the two equations for ϕ_1^{n+1} and ϕ_2^{n+1} in (1.7) are different only on the right-hand side. This motivates us to employ the auxiliary variable to control not only the nonlinear term $U(\phi^n)$ but also the explicit term ϕ^n, i.e., replace the temporal derivative in (1.5a) by

$$\frac{\phi^{n+1} - \frac{r^{n+1}}{\sqrt{E_1[\phi^n]+C_0}}\phi^n}{\Delta t}.$$

Consequently, this gives rise to the counterpart of (1.6):

$$(I + \Delta t\mathcal{G}\mathcal{L})\phi^{n+1} = r^{n+1}\left(\frac{\phi^n}{\sqrt{E_1[\phi^n]+C_0}} - \Delta t\mathcal{G}\left(\frac{U[\phi^n]}{\sqrt{E_1[\phi^n]+C_0}}\right)\right), \tag{2.1}$$

which requires only the solution of the *single* equation

$$(I + \Delta t\mathcal{G}\mathcal{L})\bar{\phi}^{n+1} = \frac{\phi^n}{\sqrt{E_1[\phi^n]+C_0}} - \Delta t\mathcal{G}\left(\frac{U[\phi^n]}{\sqrt{E_1[\phi^n]+C_0}}\right) \tag{2.2}$$

and then to determine ϕ^{n+1} and r^{n+1} from $\phi^{n+1} = r^{n+1}\bar{\phi}^{n+1}$ and (1.5c).

However, such a naive treatment on the temporal derivative term could not lead to even first-order convergence due to the fact that

$$\frac{\phi^{n+1} - \frac{r^{n+1}}{\sqrt{E_1[\phi^n]+C_0}}\phi^n}{\Delta t}$$

is no longer a first-order approximation of $\frac{\partial\phi}{\partial t}\big|^{n+1}$. Specifically, assuming that r^{n+1} is approximated such that $\frac{r^{n+1}}{\sqrt{E_1[\phi^n]+C_0}} = 1 + \mathcal{O}(\Delta t)$, we have

$$\frac{\phi^{n+1} - \xi^{n+1}\phi^n}{\Delta t} = \frac{\phi^{n+1} - \phi^n}{\Delta t} + \frac{1-\xi^{n+1}}{\Delta t}\phi^n = \frac{\partial\phi}{\partial t}\Big|^{n+1} + \mathcal{O}(\phi^n), \tag{2.3}$$

where $\xi^{n+1} := \frac{r^{n+1}}{\sqrt{E_1[\phi^n]+C_0}}$. Actually, in order to achieve first-order approximation of $\frac{\partial\phi}{\partial t}\big|^{n+1}$ using the novel formula (2.3), ξ^{n+1} needs to be approximated such that $\xi^{n+1} = 1 + \mathcal{O}(\Delta t^k)$, $k \geq 2$.

This inspires us to replace the controlling factor $\xi^{n+1} = \frac{r^{n+1}}{\sqrt{E_1[\phi^n]+C_0}}$ by

$$\theta + (1-\theta)\xi^{n+1}, \tag{2.4}$$

where θ is a given constant such that $\theta = 1 + \mathcal{O}(\Delta t)$. In this way, it is direct to observe that

$$\frac{\phi^{n+1} - [\theta + (1-\theta)\xi^{n+1}]\phi^n}{\Delta t} = \frac{\phi^{n+1}-\phi^n}{\Delta t} + \frac{(1-\theta)(1-\xi^{n+1})}{\Delta t}\phi^n = \frac{\partial \phi}{\partial t}\Big|^{n+1} + \mathcal{O}(\Delta t). \tag{2.5}$$

More generally, for any $\theta = 1 + \mathcal{O}(\Delta t^m)$ and $\xi^{n+1} = 1 + \mathcal{O}(\Delta t^n)$, we have

$$\theta + (1-\theta)\xi^{n+1} = 1 + \mathcal{O}(\Delta t^{n+m}). \tag{2.6}$$

This observation makes it possible to achieve high-order convergence of ϕ^{n+1} with lower-order approximation for ξ^{n+1}.

The novel approximation (2.5) brings about significant issues in devising energy-stable schemes. In order to overcome this obstacle, we adopt some ideas from the recently proposed generalized positive auxiliary variable method in [28]. Specifically, in [28] it is suggested to (i) use a shifted total energy $E[\phi] = E_{tot}[\phi] + C_0$ instead of $E_1[\phi]$ in (1.3) to define the SAV; (ii) use the energy balance equation of the gradient flow (1.1) instead of (1.4) to construct the dynamical equation of the auxiliary variable, i.e., we adopt the following equation as the dynamical equation:

$$\frac{dE[\phi]}{dt} = \int_\Omega \frac{\delta E}{\delta \phi}\frac{\partial \phi}{\partial t} d\Omega = -\left(\frac{\delta E}{\delta \phi}, \mathcal{G}\frac{\delta E}{\delta \phi}\right) = -(\mu, \mathcal{G}\mu) \le 0; \tag{2.7}$$

and (iii) use a delicate treatment of the dynamical equation to preserve the positiveness of the auxiliary variable in the discrete level. With the help of these intuitive thoughts, we are ready to construct new unconditionally energy-stable schemes, which require solving only one linear equation with constant coefficients at each time step.

We define a shifted total energy by

$$E[\phi] = E_{tot}[\phi] + C_0 = \frac{1}{2}(\phi, \mathcal{L}\phi) + E_1(\phi) + C_0, \tag{2.8}$$

where C_0 is a chosen scalar such that $E[\phi] > 0$ for all ϕ. Note that for a physically meaningful system, the total energy E_{tot} is bounded from below; thus such a C_0 is always available. In the spirit of the recent work [28], we introduce an SAV $R(t) := E[\phi]$, which satisfies the following dynamical equation:

$$\frac{dR(t)}{dt} = \frac{dE[\phi]}{dt} = -(\mu, \mathcal{G}\mu). \tag{2.9}$$

Define $\xi(t) = \frac{R(t)}{E(t)}$ and note that $\xi(t) \equiv 1$ at the continuous level, we can reformulate the system (1.1)–(1.2) into the following equivalent form:

$$\frac{\partial \phi}{\partial t} = -\mathcal{G}\mu, \tag{2.10a}$$

$$\mu = \mathcal{L}\phi + [\theta + (1-\theta)\xi]U[\phi], \tag{2.10b}$$

$$\frac{dR}{dt} = -\xi(\mu, \mathcal{G}\mu), \tag{2.10c}$$

where $\theta(t)$ can be an arbitrary function at the continuous level. Our new first-order scheme for (2.10) is as follows:

$$\frac{\phi^{n+1}-[\theta^n+(1-\theta^n)\xi^{n+1}]\phi^n}{\Delta t}=-\mathcal{G}\mu^{n+1}, \tag{2.11a}$$

$$\mu^{n+1}=\mathcal{L}\phi^{n+1}+[\theta^n+(1-\theta^n)\xi^{n+1}]U(\phi^n), \tag{2.11b}$$

$$\xi^{n+1}=\frac{R^{n+1}}{E[\bar{\phi}^{n+1}]}, \tag{2.11c}$$

$$\frac{R^{n+1}-R^n}{\Delta t}=-\xi^{n+1}\left(\bar{\mu}^{n+1},\mathcal{G}\bar{\mu}^{n+1}\right), \tag{2.11d}$$

where θ^n, $\bar{\phi}^{n+1}$ and $\bar{\mu}^{n+1}$ are to be specified below, together with the initial conditions

$$\phi^0=\phi_0(\boldsymbol{x},t),\quad R^0=E[\phi_0]. \tag{2.12}$$

Combining (2.11a) and (2.11b) leads to the following linear equation:

$$\big(I+\Delta t\mathcal{G}\mathcal{L}\big)\phi^{n+1}=\big(\theta^n+(1-\theta^n)\xi^{n+1}\big)\Big(\phi^n-\Delta t\mathcal{G}\big(U[\phi^n]\big)\Big). \tag{2.13}$$

Setting

$$\phi^{n+1}=\big(\theta^n+(1-\theta^n)\xi^{n+1}\big)\bar{\phi}^{n+1} \tag{2.14}$$

in the above, we find that $\bar{\phi}^{n+1}$ is determined by

$$\big(I+\Delta t\mathcal{G}\mathcal{L}\big)\bar{\phi}^{n+1}=\phi^n-\Delta t\mathcal{G}\big(U[\phi^n]\big). \tag{2.15}$$

Once $\bar{\phi}^{n+1}$ is known, we define

$$\bar{\mu}^{n+1}=\mathcal{L}\bar{\phi}^{n+1}+U(\bar{\phi}^{n+1}). \tag{2.16}$$

Note that $\bar{\phi}^{n+1}$ can be viewed as an approximation of $\phi(t^{n+1})$ by a direct semi-implicit method. Thus, $\bar{\phi}^{n+1}$ and $\bar{\mu}^{n+1}$ are first-order approximations of ϕ^{n+1} and μ^{n+1}. Inserting (2.11c) into (2.11d) leads to

$$\xi^{n+1}=\frac{R^n}{E[\bar{\phi}^{n+1}]+\Delta t(\bar{\mu}^{n+1},\mathcal{G}\bar{\mu}^{n+1})}. \tag{2.17}$$

It remains to specify θ^n which should be chosen such that $\theta^n=1+\mathcal{O}(\Delta t)$ for first-order consistency. While theoretically, $\theta^n=1+\mathcal{O}(\Delta t)$ suffices to have the desired order of accuracy and leads to stable schemes, our numerical results indicate that $\theta^n=\xi^n$, which obviously satisfies the order requirement, leads to more accurate and robust results.

To summarize, the scheme (2.11a)–(2.11d) can be implemented as follows:

- solve $\bar{\phi}^{n+1}$ from (2.15);
- set $\bar{\mu}^{n+1}=\mathcal{L}\bar{\phi}^{n+1}+U(\bar{\phi}^{n+1})$ and compute ξ^{n+1} from (2.17);
- update $\phi^{n+1}=\big(\theta^n+(1-\theta^n)\xi^{n+1}\big)\bar{\phi}^{n+1}$ and go to the next time step.

We observe that the above procedure only requires solving one linear equation with constant coefficients as in a standard semi-implicit scheme. As for the stability, we have the following result.

THEOREM 2.1. *Given $R^n\geq 0$, we have R^{n+1}, $\xi^{n+1}\geq 0$, and the scheme* (2.11a)–(2.11d) *is unconditionally energy stable in the sense that*

$$R^{n+1}-R^n=-\Delta t\xi^{n+1}\left(\bar{\mu}^{n+1},\mathcal{G}\bar{\mu}^{n+1}\right)\leq 0. \tag{2.18}$$

Proof. In light of (2.7), $(\bar{\mu}^{n+1},\mathcal{G}\bar{\mu}^{n+1})\geq 0$. Given that $R^n\geq 0$, since $E[\bar{\phi}^{n+1}]>0$, we derive from (2.17) that $\xi^{n+1}\geq 0$. We then conclude from (2.11d). ∎

3. Extension to higher order. The proposed method can be extended to construct high-order unconditionally energy-stable schemes when coupled with k-step BDF (BDFk). The essential idea is that we can achieve overall kth-order accuracy for ϕ by using just a first-order approximation for ξ if we choose θ^n such that $\theta^n + (1-\theta^n)\xi^{n+1}$ is a $(k+1)$th-order approximation to 1, thanks to (2.5). Actually, for any $\theta^n = 1 + \mathcal{O}(\Delta t^p)$ and $\xi^{n+1} = 1 + \mathcal{O}(\Delta t^q)$, we have that

$$\theta^n + (1-\theta^n)\xi^{n+1} = 1 + \mathcal{O}(\Delta t^{p+q}). \tag{3.1}$$

3.1. A recurrence formula for $\boldsymbol{\theta^n}$. As discussed in the first-order case, the proposed scheme tends to be more accurate and robust when θ^n is computed from ξ^n. In what follows, we provide a recurrence formula to effectively construct θ^n from ξ^n such that $\theta^n + (1-\theta^n)\xi^{n+1}$ is sufficient to achieve kth-order convergent scheme for ϕ at t^{n+1}.

Given ξ^n and letting l be an integer to be specified, we define θ^n by the following recursion:

$$\begin{aligned} &\gamma_0 = \xi^n + (1-\xi^n)\xi^n, \\ &\gamma_1 = \gamma_0 + (1-\gamma_0)\gamma_0, \\ &\gamma_2 = \gamma_1 + (1-\gamma_1)\gamma_1, \\ &\cdots \\ &\theta^n = \gamma_l = \gamma_{l-1} + (1-\gamma_{l-1})\gamma_{l-1}. \end{aligned} \tag{3.2}$$

One can easily check that the following result holds.

LEMMA 3.1. *If ξ^n and ξ^{n+1} are first-order approximations to* 1, *i.e.,* ξ^n, $\xi^{n+1} = 1 + \mathcal{O}(\Delta t)$, *then*

$$\theta^n + (1-\theta^n)\xi^{n+1} = 1 + \mathcal{O}\left(\Delta t^{1+2^{l+1}}\right), \tag{3.3}$$

where θ^n is obtained by (3.2).

Thus, to achieve an overall kth-order scheme for ϕ, it suffices to choose the smallest nonnegative integer l satisfying

$$l \geq \frac{\ln k}{\ln 2} - 1. \tag{3.4}$$

For example, for $k = 2, 3, 4$, l can be chosen as $0, 1, 1$, respectively.

3.2. A *k*th-order energy-stable scheme. Combining the idea from the previous section for the first-order scheme, the above recurrence relation for constructing θ^n, and the classical BDFk, we arrive at a new kth-order BDFk scheme:

$$\frac{\alpha\phi^{n+1} - [\theta^n + (1-\theta^n)\xi^{n+1}]\hat{\phi}^n}{\Delta t} = -\mathcal{G}\mu^{n+1}, \tag{3.5a}$$

$$\mu^{n+1} = \mathcal{L}\phi^{n+1} + [\theta^n + (1-\theta^n)\xi^{n+1}]U\left(\phi^{*,n+1}\right), \tag{3.5b}$$

$$\xi^{n+1} = \frac{R^{n+1}}{E[\bar{\phi}^{n+1}]}, \tag{3.5c}$$

$$\frac{R^{n+1} - R^n}{\Delta t} = -\xi^{n+1}\left(\bar{\mu}^{n+1}, \mathcal{G}\bar{\mu}^{n+1}\right), \tag{3.5d}$$

where θ^n is obtained from (3.2). Here, α, $\hat{\phi}^n$, and $\phi^{*,n+1}$ in (3.5) are defined as follows:

BDF2:

$$\alpha = \frac{3}{2}, \quad \hat{\phi}^n = 2\phi^n - \frac{1}{2}\phi^{n-1}, \quad \phi^{*,n+1} = 2\phi^n - \phi^{n-1}; \tag{3.6}$$

BDF3:

$$\alpha = \frac{11}{6}, \quad \hat{\phi}^n = 3\phi^n - \frac{3}{2}\phi^{n-1} + \frac{1}{3}\phi^{n-2}, \quad \phi^{*,n+1} = 3\phi^n - 3\phi^{n-1} + \phi^{n-2}; \tag{3.7}$$

BDF4:

$$\begin{aligned} &\alpha = \frac{25}{12}, \quad \hat{\phi}^n = 4\phi^n - 3\phi^{n-1} + \frac{4}{3}\phi^{n-2} - \frac{1}{4}\phi^{n-3}, \\ &\phi^{*,n+1} = 4\phi^n - 6\phi^{n-1} + 4\phi^{n-2} - \phi^{n-3}. \end{aligned} \tag{3.8}$$

We can also use BDF5 and BDF6, but for the sake of brevity, we omit the detailed formula here.

Note that the solution algorithm for the new BDFk scheme is the same as the first-order scheme presented in section 2. In each time step, it requires only the solution of one linear equation with constant coefficients, making the proposed method highly efficient. The new BDFk scheme also enjoys the same stability as the first-order scheme, namely, we can prove the following result using exactly the same procedure as in section 2.

THEOREM 3.2. *Given $R^n \geq 0$, we have R^{n+1}, $\xi^{n+1} \geq 0$, and the scheme* (3.5a)–(3.5d) *for any $k \geq 2$ is unconditionally energy stable in the sense that*

$$R^{n+1} - R^n = -\Delta t \xi^{n+1} \left(\bar{\mu}^{n+1}, \mathcal{G}\bar{\mu}^{n+1}\right) \leq 0. \tag{3.9}$$

Remark 3.1. Note that the stability is built into the scheme in (3.5d), independent of the actual scheme used in (3.5a) and (3.5b). In principle, we can use any linear multistep schemes in place of (3.5a) and (3.5b).

4. Adaptive time-stepping strategy for SAV BDFk schemes. To achieve satisfactory numerical results in real simulations efficiently, we are supposed to use small time steps when the energy and solution of gradient flows vary drastically while using relatively larger time steps when they vary slightly. However, for conditionally stable schemes, the allowable time step is often dictated by the stability constraint, not by accuracy. One salient feature of an unconditionally energy-stable scheme is that it allows us to employ an appropriate adaptive time-stepping strategy [9, 17, 21, 31]. Note that time-adaptivity strategy has been applied to first-order and second-order Crank–Nicolson SAV schemes in [11, 19, 24]. There are essential difficulties in applying adaptive time-stepping to other schemes, particularly other second- or higher-order schemes. The main reason is that one does not have robust unconditionally stable second- or higher-order schemes with variable step sizes. In a recent work [9], the authors developed a stabilized second-order BDF scheme with variable step sizes that is stable if $\tau^{n+1} \leq \gamma^* \tau^n$, where $\{\tau^k\}$ are the time step sizes and $\gamma^* \approx 1.5$ for optimal convergence. To the best of our knowledge, there is no unconditionally stable third- or higher-order BDF scheme with variable step sizes.

However, as stated in Remark 3.1, we can replace (3.5a) and (3.5b) by any linear multistep schemes without affecting the stability provided by (3.9). In particular, we can replace them by the BDFk schemes (along with kth-order extrapolation formula for nonlinear terms) with variable step sizes which we shall derive in the appendix.

It is crucial to figure out a good indicator for adaptive time-stepping schemes, which suggests that we adjust the time step at reasonable moments. Some observations from abundant numerical experiments are as follows:

(i) to achieve an accurate result, ξ^{n+1} has to be a good approximation to 1;
(ii) ξ^{n+1} starts to deviate from 1 when oscillation or inaccuracy tends to happen, while adopting a smaller time step can avoid such a situation.

These observations suggest to us that $|1-\xi^{n+1}|$ is a suitable indicator for the time-adaptivity procedure. Roughly speaking, we should decrease the time step whenever $|1-\xi^{n+1}|$ is bigger than a given tolerance while we can maintain a relatively large time step whenever $|1-\xi^{n+1}|$ is small enough.

Based on these observations, we provide an adaptive time-stepping algorithm for the proposed BDFk SAV scheme. Given a default safety coefficient ρ, a reference tolerance tol, the minimum time steps $\tau_{\min}$ and the maximum time steps $\tau_{\max}$, and the adaptivity speed tunable constant r, we can update the time step size by the following formula:

$$A_{dp}(e,\tau) = \rho\Big(\frac{tol}{e}\Big)^r \tau. \tag{4.1}$$

The corresponding algorithm is summarized as follows.

Algorithm 1. Time step adaptive procedure.
Given: the previous time step τ_n.
step 1. compute ξ^n from previous step with time step τ_n;
step 2. calculate $e_n = |1-\xi^n|$;
step 3. if $e_n > tol$, **then**
recalculate time step $\tau_n \leftarrow \max\{\tau_{\min}, \min\{A_{dp}(e_n,\tau_n), \tau_{\max}\}\}$;
goto step 1
step 4. else update time step $\tau_{n+1} \leftarrow \max\{\tau_{\min}, \min\{A_{dp}(e_n,\tau_n), \tau_{\max}\}\}$;
step 5. endif

Remark 4.1. It is suggested in [34] that when R^n has an obvious deviation from $E[\phi^n]$, a reset of $R^n = E[\phi^n]$ can be prescribed to improve the long time accuracy of the numerical scheme. This strategy could also be incorporated into the time-adaptivity algorithm. Specifically, R^n is reset to $E[\phi^n]$ when τ_{n+1}/τ_n is less than a threshold value.

The proposed time-stepping strategy will be applied to the simulations of Allen–Cahn and Cahn–Hilliard equations in the next section to show its advantages to achieve high accuracy with low computational cost.

5. Representative numerical examples. In this section, we provide ample numerical results to validate the accuracy and efficiency of our proposed method. Comparisons with the original SAV approach [23, 24] will be reported, and the efficiency of the time-adaptivity technique for high-order schemes will be addressed.

Let us consider two typical types of gradient flow, i.e., the Allen–Cahn equation [1] and the Cahn–Hilliard equation [6, 7]. Given the free energy

$$E_{tot}[\phi] = \int_\Omega \frac{\lambda}{2}|\nabla\phi|^2 + E_1[\phi]d\Omega, \quad E_1[\phi] = \frac{\lambda}{4\eta^2}(1-\phi^2)^2, \tag{5.1}$$

the chemical potential in (1.2) takes the form

$$\mu = \frac{\delta E_{tot}}{\delta\phi} = -\lambda\nabla^2 + U[\phi], \quad U[\phi] = \frac{\lambda}{\eta^2}\phi(\phi^2-1). \tag{5.2}$$

The Allen–Cahn equation corresponds to the L^2 gradient flow with $\mathcal{G} = m_0 I$, while the Cahn–Hilliard equation corresponds to the H^{-1} gradient flow with $\mathcal{G} = -m_0\nabla^2$ in (1.1).

Remark 5.1. Although we consider only the Allen–Cahn and the Cahn–Hillard equations in the forthcoming numerical experiments, it is worthwhile to point out that our proposed approach is directly applicable to gradient flow problems where the nonlinear part of the free energy contains spatial derivatives, e.g., the molecular beam epitaxy model [11].

Example 1 (convergence rate of the new SAV/BDFk scheme for the Allen–Cahn and Cahn–Hilliard equations). Consider the Allen–Cahn and Cahn–Hilliard equations in the computational domain $\Omega = [0, 2] \times [0, 2]$ with a contrived exact solution

$$\phi(\boldsymbol{x}, t) = \cos(\pi x)\cos(\pi y)\sin(t)/(1 + 10t^2) \tag{5.3}$$

and, correspondingly, the external source term $f(\boldsymbol{x}, t)$ satisfying $\phi_t = -\mathcal{G}\mu + f$. The Fourier spectral method [25] for spatial discretization is employed throughout this section. N_x and N_y denote the number of Fourier collocation points along the x and y axis, respectively. In the simulations, we set $(N_x, N_y) = (40, 40)$ with which the spatial discretization error is negligible compared with time discretization error. Other parameters are $\lambda = 0.01$, $m_0 = 0.01$, $\eta = 0.05$, and $C_0 = 0$. The algorithm for the new SAV/BDFk ($k = 1, 2, 3, 4$) is employed to numerically integrate the governing equations in time from $t = 0.1$ to $t = 1.1$. The L^2 errors of ϕ at $t = 1.1$ are plotted, respectively, in Figure 5.1(a)–(b) for the Allen–Cahn equation and Figure 5.2(a)–(b) for the Cahn–Hilliard equation, where we can observe the expected convergence rate of the field variable ϕ for all cases.

Recall that $R(t) = E[\phi]$ in the continuous level, and the evolution equation of $R(t)$ stems from this equation. The discretization (3.5d) of $R(t)$ leads to a first-order approximation of $E[\phi]$. Consequently, $\xi^{n+1} = \frac{R^{n+1}}{E[\phi^{n+1}]}$ is a first-order approximation of 1. We depict the L^∞ error of ξ^{n+1} to 1 for the Allen–Cahn and Cahn–Hilliard equations in Figure 5.1(c)–(d) and Figure 5.2(c)–(d), respectively. As expected, it can be observed that ξ^{n+1} converges to 1 with a first-order convergence rate for all cases. Moreover, this observation implies that ξ^{n+1} can serve as an indicator of the accuracy of the simulations. If the difference of ξ^{n+1} from 1 is small, then the simulation tends to be more accurate. Otherwise, when ξ^{n+1} deviates significantly from 1, the simulation is no longer accurate.

Example 2 (spinodal decomposition for the Allen–Cahn equation). Consider the spinodal decomposition of a homogeneous mixture into two coexisting phases governed by the Allen–Cahn equation as another test of the algorithms developed herein. The computational domain is $[0, 2] \times [0, 2]$, and the initial phase field is given by uniformly distributed data between $[-0.5, 0.5]$. We adopt $(N_x, N_y) = (512, 512)$, $\lambda = 1$, $m_0 = 10^{-4}$, $\eta = 0.005$, and $C_0 = 0$ in the forthcoming simulations. The new SAV/BDF2 scheme is employed to numerically integrate this problem.

In Figure 5.3, we depict a temporal sequence of snapshots of the interfaces formed between the two phases. Figure 5.4 shows the time histories of the total energy $E_{tot}[\phi]$ obtained by the current method and the original SAV method using various time steps $\Delta t = 10^{-1}, 10^{-2}, 10^{-3}$. A reference solution obtained with $\Delta t = 10^{-4}$ using the original SAV scheme is also included for comparison. It can be observed in Figure 5.4(a) that all the energy history curves decrease dramatically at the beginning and level off gradually, indicating the stability of the proposed method. In Figure 5.4(b),

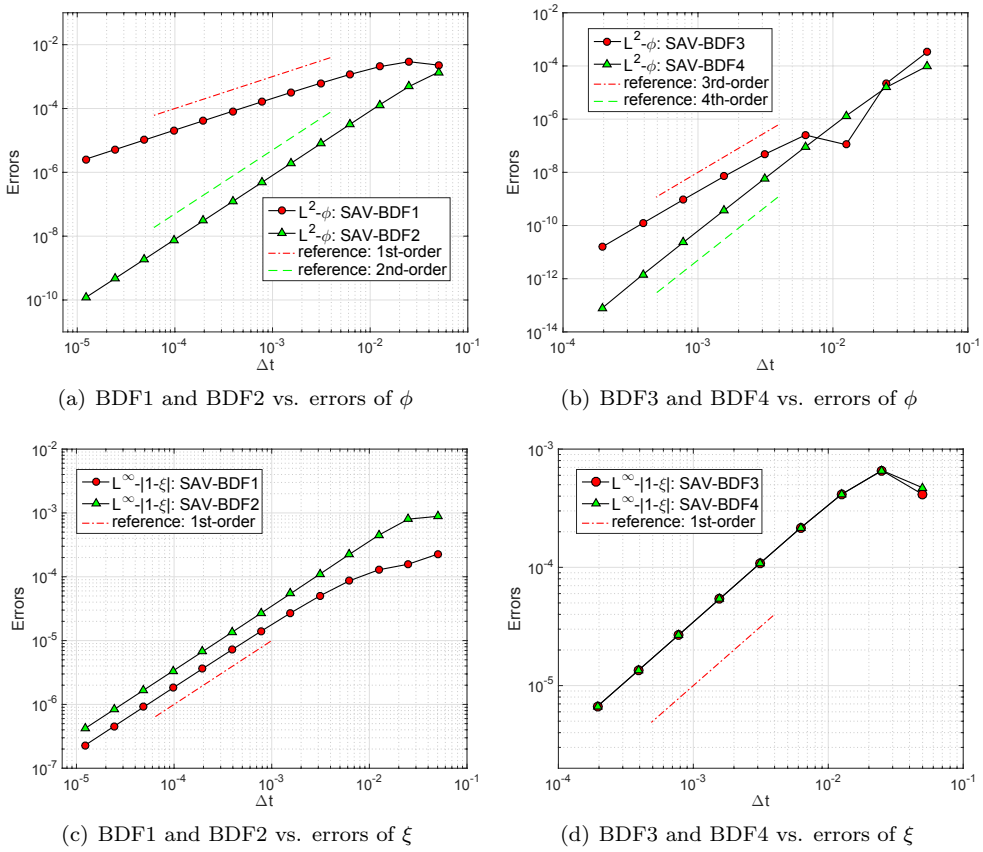

(a) BDF1 and BDF2 vs. errors of ϕ

(b) BDF3 and BDF4 vs. errors of ϕ

(c) BDF1 and BDF2 vs. errors of ξ

(d) BDF3 and BDF4 vs. errors of ξ

FIG. 5.1. *(Example 1.) Temporal convergence test for the Allen–Cahn equation using the new SAV/BDFk* ($k = 1, 2, 3, 4$). (a)–(b) L^2 *errors of* ϕ *as a function of* Δt*;* (c)–(d) L^∞ *errors of* ξ *as a function of* Δt.

we zoom in the energy history curves at the region $t \in [0, 0.1]$. It shows that the results obtained by the current method and the original SAV method overlap with each other for the same time step size. This implies that the proposed method provides almost the same accuracy as the original SAV method, but with halved computational cost. It also indicates that to achieve acceptable accuracy, the step size should be chosen no bigger than $\Delta t = 10^{-3}$.

Example 3 (application of adaptive time-stepping strategy to Example 2). Next, we use the spinodal decomposition governed by the Allen–Cahn equation to demonstrate the performance of the time adaptivity. The setup is the same as in Example 2. The proposed SAV/BDFk schemes with variable time steps using $l = 0, 1, 1$ in the recurrence relation (3.2) for $k = 2, 3, 4$, respectively, are employed to numerically integrate this problem. We choose $\rho = 0.9$, $tol = 10^{-3}$, and $r = 0.25$ in (4.1). The minimum time step is taken as $\tau_{\min} = 10^{-6}$, while the maximum time step is take as $\tau_{\max} = 10^{-3/k}$, $k = 2, 3, 4$, respectively, such that when $\tau_{\max}$ is employed, the errors for BDFk schemes ($k = 2, 3, 4$) are of the same level. The initial time step is taken as $\tau_{\min}$.

In Figure 5.5(a), we depict the energy history curves obtained by BDFk ($k = 2, 3, 4$) schemes for long time simulations, and it can be seen that the curves essentially overlap with each other. Correspondingly, the snapshots of the interfaces between

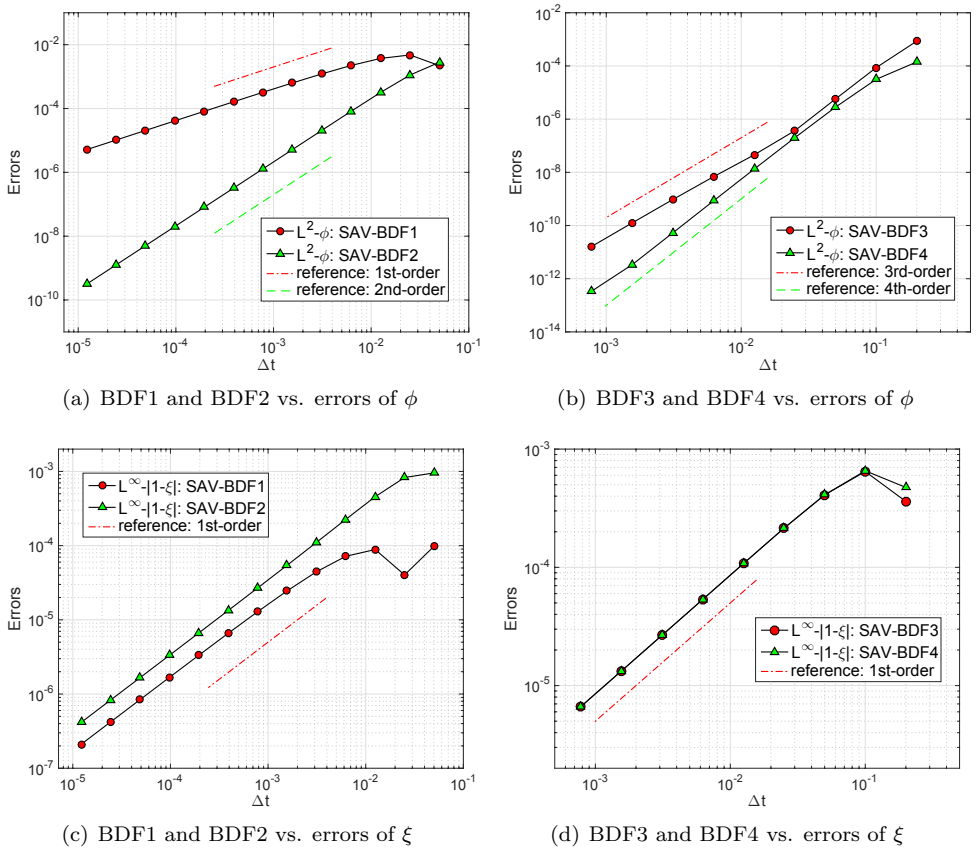

(a) BDF1 and BDF2 vs. errors of ϕ

(b) BDF3 and BDF4 vs. errors of ϕ

(c) BDF1 and BDF2 vs. errors of ξ

(d) BDF3 and BDF4 vs. errors of ξ

FIG. 5.2. *(Example 1.) Temporal convergence test for the Cahn–Hilliard equation using the new SAV/BDFk* ($k = 1, 2, 3, 4$). (a)–(b) L^2 *errors of* ϕ *as a function of* Δt*;* (c)–(d) L^∞ *errors of* ξ *as a function of* Δt.

these two phases at $t = 300$ are compared in Figure 5.5(b)–(d), and no noticeable difference can be observed.

In order to demonstrate the efficiency of the time-adaptivity technique, we plot in Figures 5.6, 5.7, and 5.8 the time history curves of the time steps and time step ratios between two successive steps in the time window $t \in (0, 3)$, where rapid changes of the phase field variable occur. It can be seen that the time steps gradually increase for all these three solvers, and the average time steps in these period are 1.6×10^{-2}, 2.0×10^{-2}, and 2.1×10^{-2}. Note that in Example 2, for the BDF2 scheme with a fixed time step, it takes at least $\Delta t = 10^{-3}$ to obtain reasonable numerical results. We also record the total wall time of this simulation computed from $t = 0$ to $t = 300$ with the BDF2 scheme using a fixed time step $\Delta t = 10^{-3}$, which is 19970.2 seconds. While equipped with the time-adaptivity technique, the total wall time for the BDF2–BDF4 schemes reduces drastically to 929.0 seconds, 318.9 seconds, and 429.6 seconds, respectively. The speedups in these simulations are noticeable, compared with the solver without time adaptivity. In [9], it is pointed out that the variable step BDF2 scheme is stable if $\tau^{n+1} \leq \gamma^* \tau^n$ and $\gamma^* \approx 1.5$ for optimal convergence, while with the current method, we are not restricted by this constraint, and the maximum time step ratios are observed to be as large as 22, 41, 41 for $k = 2, 3, 4$.

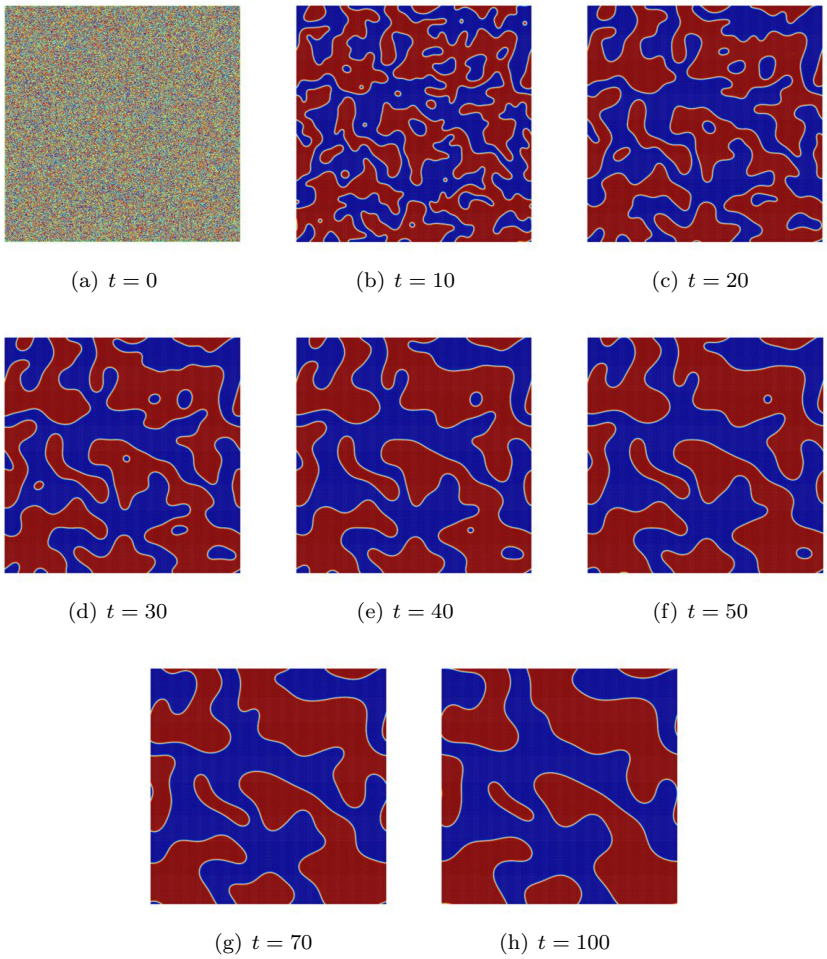

(a) $t = 0$ (b) $t = 10$ (c) $t = 20$

(d) $t = 30$ (e) $t = 40$ (f) $t = 50$

(g) $t = 70$ (h) $t = 100$

FIG. 5.3. *(Example 2.) Spinodal decomposition governed by the Allen–Cahn equation. The simulation is obtained with* $\Delta t = 10^{-3}$.

Example 4 (merging of an array of circles for the Cahn–Hilliard equation). We consider, as another test problem, the merging of a rectangular array of 9×9 circles governed by the Cahn–Hilliard equation. The computational domain is $[0, 2] \times [0, 2]$, and the initial phase field is given by

$$\phi_0(\boldsymbol{x}, t) = 80 - \sum_{i=1}^{9}\sum_{j=1}^{9} \frac{\tanh\left(\sqrt{(x - x_i)^2 + (y - y_j)^2} - R_0\right)}{\sqrt{2}\eta}, \tag{5.4}$$

where $R_0 = 0.085$, $x_i = 0.2 \times i$, and $y_j = 0.2 \times j$ for $i, j = 1, 2, \ldots, 9$. We adopt $(N_x, N_y) = (512, 512)$, $\lambda = 1$, $m_0 = 10^{-6}$, $\eta = 0.01$, and $C_0 = 0$ in the simulations.

In Figure 5.9, we plot a temporal sequence of snapshots of the interfaces formed between the two phases using the BDF3 scheme with variable time steps using $\rho = 0.95$, $tol = 10^{-3}$, $r = 0.57$, $\tau_{\min} = 10^{-6}$, and $\tau_{\max} = 10^{-1}$ in (4.1).

In order to investigate the influence of the parameter tol to the accuracy and efficiency of the new SAV/BDFk ($k = 2, 3, 4$) schemes with time adaptivity, we depict in Figure 5.10 the L^2 errors of ϕ as a function of the average of the time step sizes.

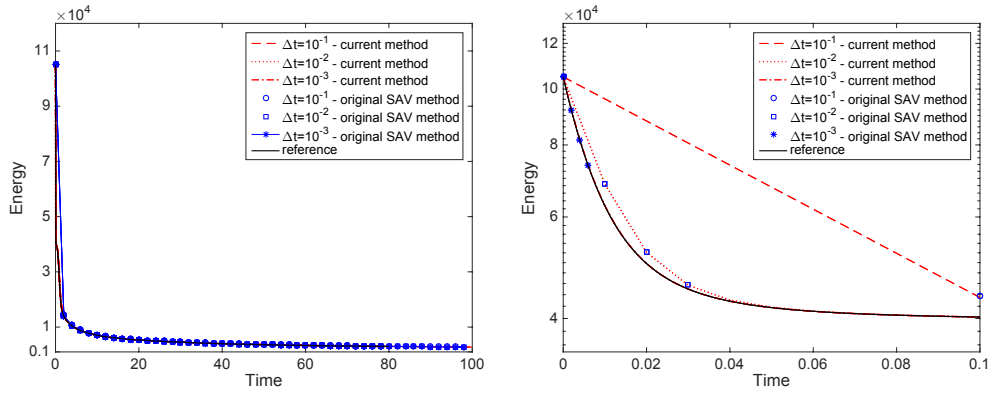

(a) Energy shown in $(0, 100)$ (b) Energy zoomed in $(0, 0.1)$

FIG. 5.4. *(Example 2.) Time histories of $E_{tot}[\phi]$ for spinodal decomposition governed by the Allen–Cahn equation obtained using the current method and the original SAV method with $\Delta t = 10^{-1}, 10^{-2}, 10^{-3}$.*

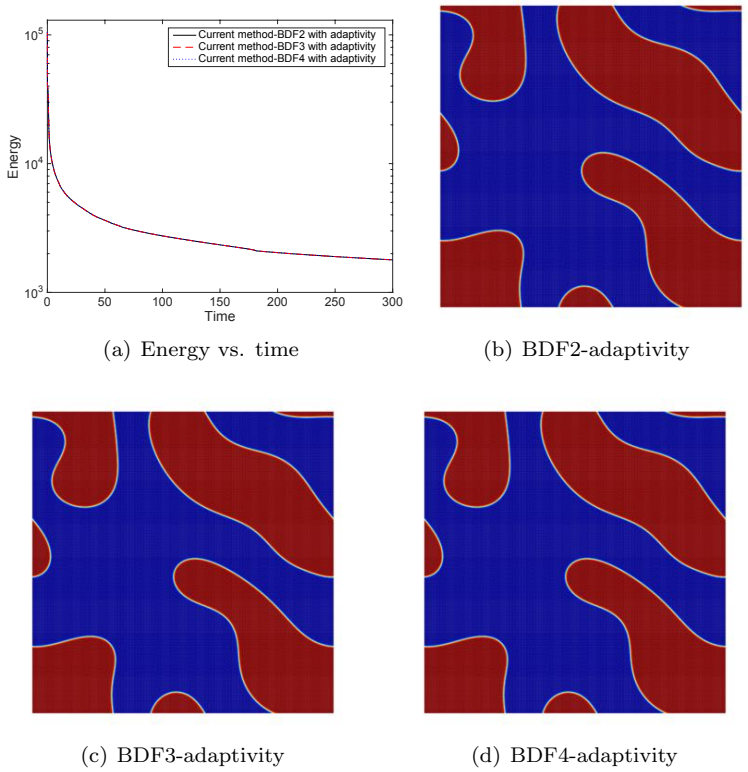

(a) Energy vs. time (b) BDF2-adaptivity

(c) BDF3-adaptivity (d) BDF4-adaptivity

FIG. 5.5. *(Example 3.) Spinoidal decomposition governed by the Allen–Cahn equation. Simulation results are obtained by the proposed SAV/BDFk ($k = 2, 3, 4$) scheme with adaptive time-stepping technique, and the snapshots* (b)–(d) *of the interfaces between these two phases are depicted at $t = 300$.*

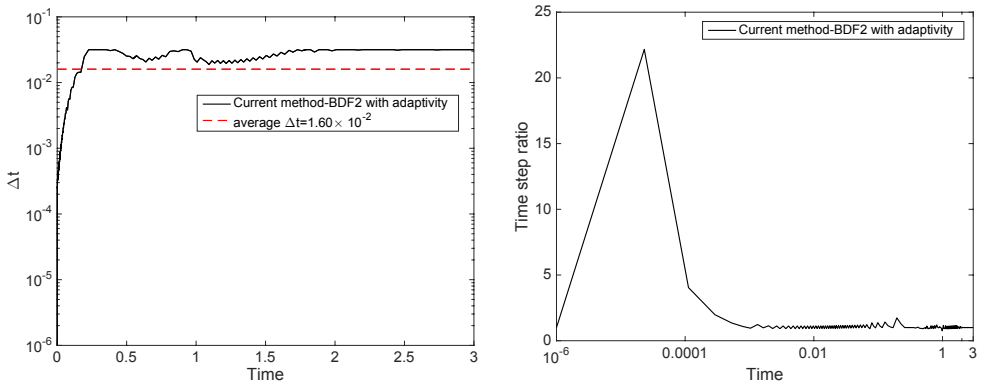

(a) History of Δt at $(0, 3)$ (b) History of τ^{n+1}/τ^n

FIG. 5.6. *(Example 3.) Time histories of time steps and time step ratios in the time window* $t \in (0, 3)$ *obtained by the BDF2 scheme with adaptive time-stepping technique. The average* $\Delta t = 1.60 \times 10^{-2}$.

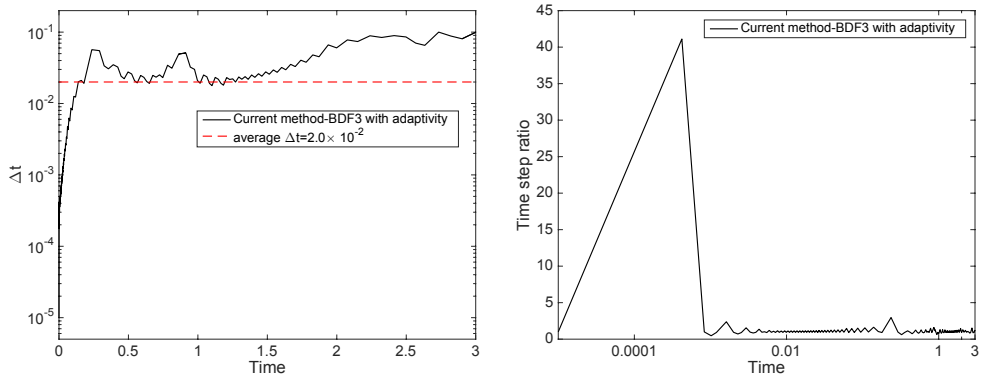

(a) History of Δt at $(0, 3)$ (b) History of τ^{n+1}/τ^n

FIG. 5.7. *(Example 3.) Time histories of time steps and time step ratios obtained by the BDF3 scheme with adaptive time-stepping technique. The average* $\Delta t = 2.0 \times 10^{-2}$.

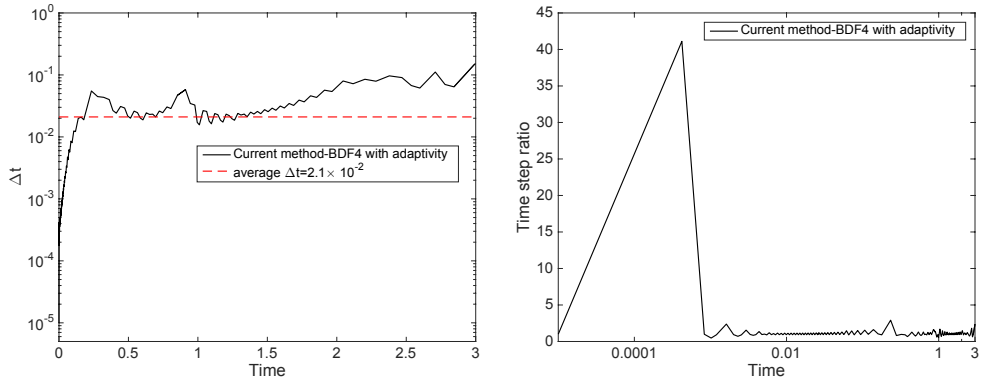

(a) History of Δt at $(0, 3)$ (b) History of τ^{n+1}/τ^n

FIG. 5.8. *(Example 3.) Time histories of time steps and time step ratios obtained by the BDF4 scheme with adaptive time-stepping technique. The average* $\Delta t = 2.1 \times 10^{-2}$.

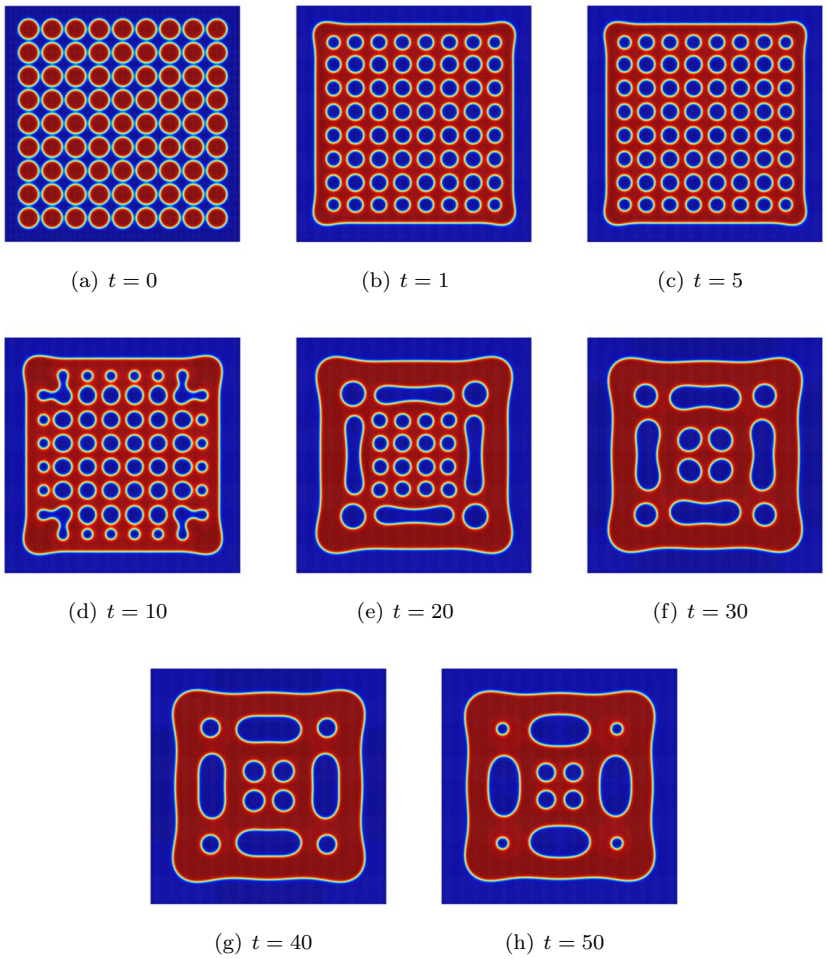

(a) $t = 0$ (b) $t = 1$ (c) $t = 5$

(d) $t = 10$ (e) $t = 20$ (f) $t = 30$

(g) $t = 40$ (h) $t = 50$

FIG. 5.9. *(Example 4.) Merging of an array of circles governed by the Cahn–Hilliard equation. Simulations are obtained with the proposed SAV/BDF3 schemes with time-adaptivity technique.*

These errors are obtained through comparing the numerical solutions with a reference solution computed by the new SAV/BDF2 scheme with a fixed small $\Delta t = 10^{-5}$ at $t = 1$. It can be seen that a better accuracy is achieved when we adopt a smaller *tol*.

Figure 5.11 is a demonstration of the stability of the proposed scheme. The time histories of the modified energy $R(t)$ obtained by large time step sizes $\Delta t = 2, 5$ are depicted. At these large time step sizes, we can no longer expect the results to be accurate. But it can be observed that the modified energy decays and remains positive for long time simulations.

In Figure 5.12, we depict a comparison of the time histories of ξ^{n+1} obtained by the new BDF2 schemes with $\theta^n = 1 - (\Delta t)^2$ and $\theta^n = \xi^n + (1 - \xi^n)\xi^n$ (see the recurrence relation (3.2)). As discussed before, the difference between ξ^{n+1} and the unit value can be used to indicate the accuracy of the computation. Thus, this comparison shows the influence of these two different choices of θ^n on the performance of the proposed scheme. It can be observed in Figure 5.12(a) that when $\Delta t = 10^{-3}$ is used, ξ^{n+1} obtained by both choices is close to 1 and the history curves of ξ^{n+1}

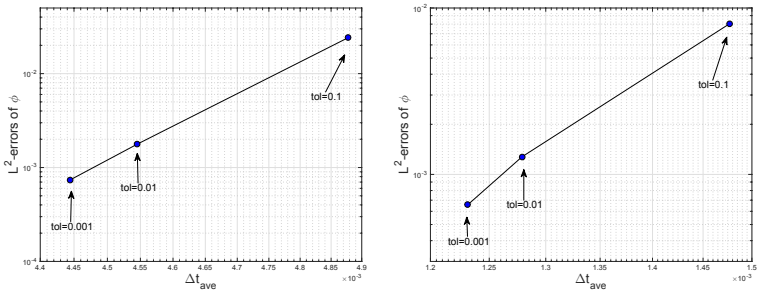

(a) BDF2 scheme with different *tol* (b) BDF3 scheme with different *tol*

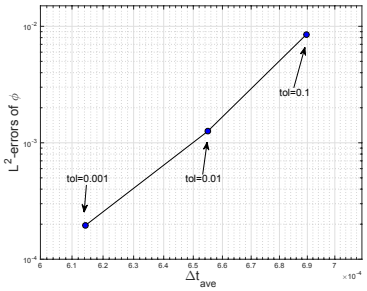

(c) BDF4 scheme with different *tol*

FIG. 5.10. *(Example 4.) L^2 errors of ϕ as a function of the average of Δt obtained by* (a) *the BDF2 scheme,* (b) *the BDF3 scheme, and* (c) *the BDF4 scheme, respectively. The time-adaptivity technique is employed with tol* $= 10^{-1}, 10^{-2}, 10^{-3}$. *The parameters* (r, ρ) *in* (4.1) *are set to be* $(0.75, 0.85)$, $(0.57, 0.95)$, $(0.7, 0.85)$ *for the BDF2–BDF4 schemes, respectively.*

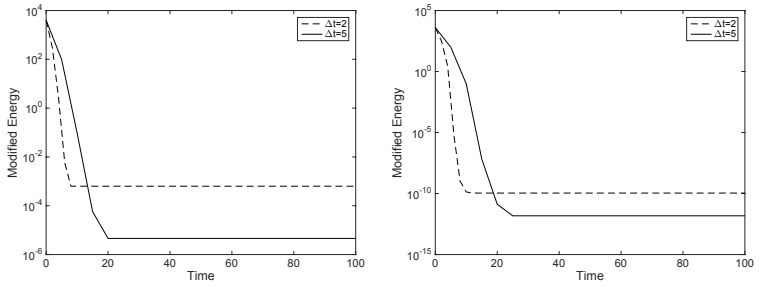

(a) BDF2 (b) BDF3

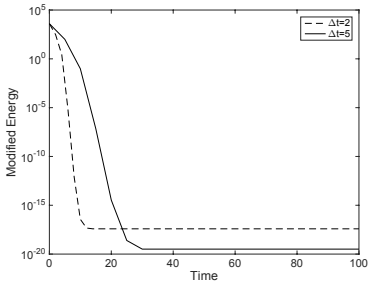

(c) BDF4

FIG. 5.11. *(Example 4.) Time histories of the modified energy $R(t)$ computed by* (a) *the BDF2 scheme,* (b) *the BDF3 scheme, and* (c) *the BDF4 scheme, using large time step sizes* $\Delta t = 2, 5$.

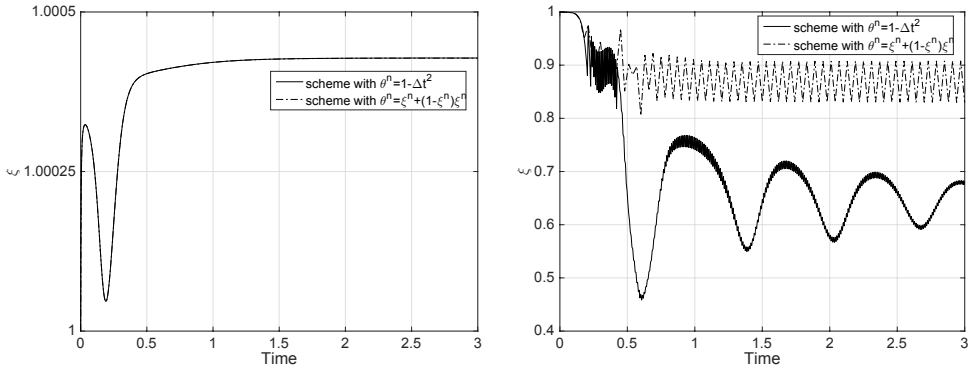

(a) History of ξ^{n+1} with $\Delta t = 10^{-3}$ (b) History of ξ^{n+1} with $\Delta t = 0.006$

FIG. 5.12. *(Example 4.) A comparison of two different choices of θ^n to the performance of the new BDF2 schemes. The time histories of ξ computed by the scheme with $\theta^n = 1 - (\Delta t)^2$ and the one with $\theta^n = \xi^n + (1 - \xi^n)\xi^n$ (see the recurrence relation (3.2)) obtained with* (a) $\Delta t = 10^{-3}$ *and* (b) $\Delta t = 0.006$.

overlap with each other, while when a relatively larger $\Delta t = 0.006$ in Figure 5.12(b) is employed, ξ^{n+1} obtained by the scheme with a constant θ^n deviates more from 1, indicating a larger numerical error, compared with the one obtained by the scheme with $\theta^n = \xi^n + (1 - \xi^n)\xi^n$.

Example 5 (an improved multiple SAV method for one-component Bose–Einstein condensates). We consider the ground state solution of one-component Bose–Einstein condensates in two dimensions [2, 3, 34] as an example to show how our current method can reduce the number of linear equations to be solved in each time step from *three* to *two*, compared with the classical multiple SAV (MSAV) [10, 34] approach.

Like [34], we consider the penalized energy

$$E(\phi) = \frac{1}{2}(\phi, \mathcal{L}\phi) + \frac{1}{2}\int_\Omega F(|\phi|)^2)d\Omega + \frac{1}{4\varepsilon}\left(\int_\Omega |\phi|^2 d\Omega - 1\right)^2. \tag{5.5}$$

Here, $F(\phi) = \frac{\beta}{2}\phi^2$, $\mathcal{L} = (-\frac{1}{2}\nabla^2 + V(x,y))\phi$ with $V(x,y) \geq 0$, and $\varepsilon \ll 1$. Correspondingly, the governing equation for this gradient flow problem takes the form

$$\frac{\partial \phi}{\partial t} = -\frac{\delta E}{\delta \phi} = -\mathcal{L}\phi - F'(|\phi|^2)\phi - \frac{1}{\varepsilon}(\|\phi\|^2 - 1)\phi \tag{5.6}$$

and is subject to the constraints

$$\int_\Omega |\phi(\boldsymbol{x}, t)|^2 d\Omega = 1, \tag{5.7a}$$

$$\lim_{|x|\to\infty} \phi(\boldsymbol{x}, t) = 0. \tag{5.7b}$$

In our new MSAV approach, we introduce two SAVs:

$$R_1(t) = E_1(\phi), \quad R_2(t) = E_2(\phi), \tag{5.8}$$

where

$$E_1 = \frac{1}{2}(\phi, \mathcal{L}\phi) + \frac{1}{2}\int_\Omega F(|\phi|)^2 d\Omega, \quad E_2 = \frac{1}{4\varepsilon}\left(\int_\Omega |\phi|^2 d\Omega - 1\right)^2. \tag{5.9}$$

With the same spirit to improve the single SAV approach in section 2, we employ one of the introduced auxiliary variables to control not only the nonlinear term, but also the explicit linear term, and consequently, we are only required to solve two linear equations at each time step. The first-order new MSAV scheme can be written as

$$\frac{\phi^{n+1}-[\theta_1^n+(1-\theta_1^n)\xi_1^{n+1}]\phi^n}{\Delta t}=-\mu^{n+1}, \tag{5.10a}$$

$$\mu^{n+1}=\mathcal{L}\phi^{n+1}+[\theta_1^n+(1-\theta_1^n)\xi_1^{n+1}]U_1(\phi^n)+[\theta_2^n+(1-\theta_2^n)\xi_2^{n+1}]U_2(\phi^n), \tag{5.10b}$$

$$\xi_1^{n+1}=\frac{R_1^{n+1}}{E_1[\bar\phi^{n+1}]},\quad \xi_2^{n+1}=\frac{R_2^{n+1}}{E_2[\bar\phi^{n+1}]}, \tag{5.10c}$$

$$\frac{R_1^{n+1}-R_1^n}{\Delta t}=-\frac{R_1^{n+1}+R_2^{n+1}}{E_1[\bar\phi^{n+1}]+E_2[\bar\phi^{n+1}]}\left(\mathcal{L}\bar\phi^{n+1}+U_1(\bar\phi^{n+1}),\bar\mu^{n+1}\right), \tag{5.10d}$$

$$\frac{R_2^{n+1}-R_2^n}{\Delta t}=-\frac{R_1^{n+1}+R_2^{n+1}}{E_1[\bar\phi^{n+1}]+E_2[\bar\phi^{n+1}]}\left(U_2(\bar\phi^{n+1}),\bar\mu^{n+1}\right), \tag{5.10e}$$

where $\bar\mu^{n+1}=\mathcal{L}\bar\phi^{n+1}+U_1(\bar\phi^{n+1})+U_2(\bar\phi^{n+1})$, $\theta_i=1+\mathcal{O}(\Delta t)$ for $i=1,2$, $\bar\phi^{n+1}$ is defined as in the single SAV case, and

$$U_1(\phi)=F'(|\phi|^2)\phi,\quad U_2(\phi)=\frac{1}{\varepsilon}(\|\phi\|^2-1)\phi. \tag{5.11}$$

The initial condition is chosen as

$$\phi_0(x,y)=\frac{(\gamma_x\gamma_y)^{1/4}}{\pi^{1/2}}e^{-(\gamma_x x^2+\gamma_y y^2)/2} \tag{5.12}$$

with two different potential functions:

Case 1. A harmonic oscillator potential

$$V(x,y)=\frac{1}{2}\left(\gamma_x^2x^2+\gamma_y^2y^2\right). \tag{5.13}$$

Case 2. A harmonic oscillator potential and a potential of a stirrer corresponding to a far-blue detuned Gaussian laser beam

$$V(x,y)=\frac{1}{2}\left(\gamma_x^2x^2+\gamma_y^2y^2\right)+\omega_0e^{-\delta((x-r_0)^2+y^2)}. \tag{5.14}$$

The parameters are chosen as $\gamma_x=1$, $\gamma_y=4$, and $\beta=200$ in Case 1 and $\gamma_x=1$, $\gamma_y=1$, $\omega_0=4$, $\delta=r_0=1$, and $\beta=200$ in Case 2. We then solve Case 1 by spectral-Galerkin method on $\Omega_1=[-8,8]\times[-4,4]$ and Case 2 on $\Omega_2=[-8,8]\times[-8,8]$. In both cases, we choose $(N_x,N_y)=(40,40)$, $\varepsilon=10^{-4}$, time steps $\Delta t=10^{-4}$ and impose the homogeneous Dirichlet boundary condition.

We plot the ground state solutions of both cases in Figure 5.13 and compare the chemical potential and the energy of the ground states with the results obtained by the original MSAV method in [34] and by the time-splitting sine-spectral (TSSP) method in [3] in Tables 1 and 2, where we denote

$$x_{\rm rms}=\|x\phi\|_{L^2(\Omega)},\quad y_{\rm rms}=\|y\phi\|_{L^2(\Omega)}, \tag{5.15}$$

and

$$\begin{aligned}\mu_\beta(\phi)&=\int_\Omega\left(\frac{1}{2}|\nabla\phi(x)|^2+V(x)|\phi(x)|^2+\beta|\phi(x)|^4\right)d\Omega\\&=E_\beta(\phi)+\int_\Omega\frac{\beta}{2}|\phi(x)|^4d\Omega.\end{aligned} \tag{5.16}$$

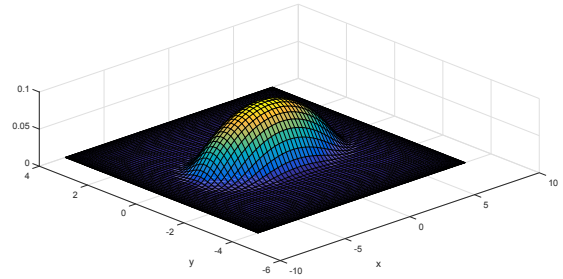

(a) Case 1

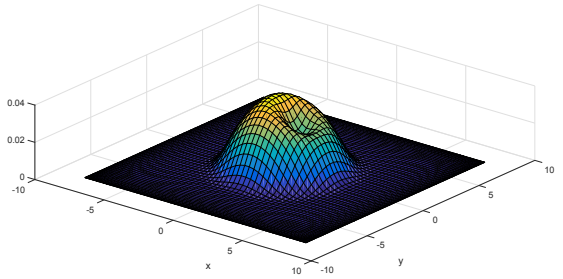

(b) Case 2

FIG. 5.13. *Ground state solutions of one-component Bose–Einstein condensates.*

TABLE 1
Case 1: $\gamma_x = 1$, $\gamma_y = 4$, and $\beta = 200$.

Case 1 of Bose–Einstein condensates				
Scheme	$x_{\rm rms}$	$y_{\rm rms}$	E_β	μ_β
TSSP	2.2734	0.6074	11.1563	16.3377
MSAV	2.2812	0.6096	11.1560	16.3002
New MSAV	2.2710	0.6064	11.1621	16.2514

TABLE 2
Case 2: $\gamma_x = 1$, $\gamma_y = 1$, $\omega_0 = 4$, $\delta = r_0 = 1$, and $\beta = 200$.

Case 2 of Bose–Einstein condensates				
Scheme	$x_{\rm rms}$	$y_{\rm rms}$	E_β	μ_β
TSSP	1.6951	1.7144	5.8507	8.3269
MSAV	1.6978	1.7169	5.8506	8.3189
New MSAV	1.6933	1.7124	5.8455	8.3202

We observe from Tables 1 and 2 that the results by our new SAV schemes are consistent with the results obtained by using the original SAV and TSSP methods.

Remark 5.2. Some remarks are in order:

1. As with the single SAV approach mentioned in section 2, one can easily prove the scheme (5.10) is unconditionally energy stable in the sense that $R_1^n + R_2^n \geq 0$ for every n and

(5.17)
$$(R_1^{n+1} + R_2^{n+1}) - (R_1^n + R_2^n) = -\Delta t \frac{R_1^{n+1} + R_2^{n+1}}{E_1[\bar{\phi}^{n+1}] + E_2[\bar{\phi}^{n+1}]} \left(\bar{\mu}^{n+1}, \bar{\mu}^{n+1}\right) \leq 0.$$

2. The new MSAV scheme (5.10) only requires solving *two* instead of *three* linear equations, compared with the original MSAV scheme in [34]. In general, if we introduce K auxiliary variables, our new MSAV scheme requires only the solution of K linear equations, while the original SAV scheme requires us to solve $K+1$ linear equations. Hence, the new MSAV scheme is more efficient.
3. We can construct higher-order unconditionally energy-stable MSAV schemes based on the approach presented in section 3.

6. Concluding remarks. We presented in this paper several essential improvements over the original SAV approach, making our new SAV approach even more efficient, flexible, and amenable to higher order. More precisely, our new SAV approach enjoys the following additional advantages:

1. For the case with single SAV, our new method only requires solving one linear equation with constant coefficients, reducing half of the computational cost of the original SAV approach. In other words, the computational cost of the new SAV approach, being unconditionally energy stable, is essentially the same as that of the semi-implicit approach which is only conditionally stable. Furthermore, the new approach does not require the nonlinear part of the free energy to be bounded from below, making it more flexible than the original SAV approach.
2. While the original SAV approach only leads to first- and second-order unconditionally stable BDF type schemes, the new SAV approach allows us to construct higher-order unconditionally energy-stable schemes with any multistep schemes. In particular, we are able to construct, for the first time, unconditionally energy-stable higher-order time adaptive schemes based on the BDFk scheme with variable step sizes.
3. For the cases where K SAVs are needed, our new method requires solving K linear equations with constant coefficients, as opposed to $K+1$ linear equations by the original MSAV approach.

The SAV method is not limited to the realm of gradient flow. The idea of introducing an SAV has been extended to many nongradient flow type problems, e.g., Navier–Stokes equation [18, 20], two phase flows [29], chemo-repulsion model [28], etc. Although we only focus on gradient flow problems in the current paper, the proposed method can be in principle extended to general dissipative systems. We will explore this issue in our future work.

Appendix A. BDF for variable time step sizes.

Given a successive of variable time steps

$$\tau^{n+1}=t^{n+1}-t^n,\quad \tau^n=t^n-t^{n-1},\quad \tau^{n-1}=t^{n-1}-t^{n-2},\quad \tau^{n-2}=t^{n-2}-t^{n-3},\dots, \tag{A.1}$$

the corresponding α, $\hat{\phi}^n$, and $\phi^{*,n+1}$ in (3.5) for BDFk scheme with kth-order extrapolation can be derived by Taylor expansion. More precisely, let us denote

$$\begin{aligned} x_1 &= -\tau^{n+1},\\ x_2 &= -\tau^{n+1}-\tau^n,\\ x_3 &= -\tau^{n+1}-\tau^n-\tau^{n-1},\\ x_4 &= -\tau^{n+1}-\tau^n-\tau^{n-1}-\tau^{n-2},\\ &\dots . \end{aligned} \tag{A.2}$$

Then, for $k=2,3,4$, the formulae are given below.

BDF2:

$$\alpha = \gamma^{-1}, \quad \hat{\phi}^n = \gamma^{-1}(a\phi^n + b\phi^{n-1}), \quad \phi^{*,n+1} = A\phi^n + B\phi^{n-1}, \tag{A.3}$$

where

$$\gamma = \frac{x_2}{x_1 + x_2}, \quad a = -\frac{x_2^2}{x_1^2 - x_2^2}, \quad b = \frac{x_1^2}{x_1^2 - x_2^2}, \tag{A.4}$$
$$A = -\frac{x_2}{x_1 - x_2}, \quad B = \frac{x_1}{x_1 - x_2}.$$

BDF3:

$$\alpha = \gamma^{-1}, \quad \hat{\phi}^n = \gamma^{-1}\left(a\phi^n + b\phi^{n-1} + c\phi^{n-2}\right), \quad \phi^{*,n+1} = A\phi^n + B\phi^{n-1} + C\phi^{n-2}, \tag{A.5}$$

where

$$\gamma = \frac{x_2\, x_3}{x_1x_2 + x_1x_3 + x_2x_3}, \quad a = \frac{x_2^2\, x_3^2}{(x_1 - x_2)(x_1 - x_3)(x_1x_2 + x_1x_3 + x_2x_3)}, \tag{A.6}$$
$$b = -\frac{x_1^2\, x_3^2}{(x_1 - x_2)(x_2 - x_3)(x_1x_2 + x_1x_3 + x_2x_3)},$$
$$c = \frac{x_1^2\, x_2^2}{(x_1 - x_3)(x_2 - x_3)(x_1x_2 + x_1x_3 + x_2x_3)},$$

and

$$A = \frac{x_2\, x_3}{(x_1 - x_2)(x_1 - x_3)}, \quad B = -\frac{x_1\, x_3}{(x_1 - x_2)(x_2 - x_3)}, \quad C = \frac{x_1\, x_2}{(x_1 - x_3)(x_2 - x_3)}. \tag{A.7}$$

BDF4:

$$\alpha = \gamma^{-1}, \quad \hat{\phi}^n = \gamma^{-1}\left(a\phi^n + b\phi^{n-1} + c\phi^{n-2} + d\phi^{n-3}\right), \tag{A.8}$$
$$\phi^{*,n+1} = A\phi^n + B\phi^{n-1} + C\phi^{n-2} + D\phi^{n-3},$$

where

$$\gamma = \frac{x_2\, x_3\, x_4}{x_1x_2x_3 + x_1x_2x_4 + x_1x_3x_4 + x_2x_3x_4}, \tag{A.9}$$
$$a = -\frac{x_2^2\, x_3^2\, x_4^2}{(x_1 - x_2)(x_1 - x_3)(x_1 - x_4)(x_1x_2x_3 + x_1x_2x_4 + x_1x_3x_4 + x_2x_3x_4)},$$
$$b = \frac{x_1^2\, x_3^2\, x_4^2}{(x_1 - x_2)(x_2 - x_3)(x_2 - x_4)(x_1x_2x_3 + x_1x_2x_4 + x_1x_3x_4 + x_2x_3x_4)},$$
$$c = -\frac{x_1^2\, x_2^2\, x_4^2}{(x_1 - x_3)(x_2 - x_3)(x_3 - x_4)(x_1x_2x_3 + x_1x_2x_4 + x_1x_3x_4 + x_2x_3x_4)},$$
$$d = \frac{x_1^2\, x_2^2\, x_3^2}{(x_1 - x_4)(x_2 - x_4)(x_3 - x_4)(x_1x_2x_3 + x_1x_2x_4 + x_1x_3x_4 + x_2x_3x_4)},$$

and

(A.10)

$$A = -\frac{x_2\, x_3\, x_4}{(x_1 - x_2)(x_1 - x_3)(x_1 - x_4)}, \quad B = \frac{x_1\, x_3\, x_4}{(x_1 - x_2)(x_2 - x_3)(x_2 - x_4)},$$
$$C = -\frac{x_1\, x_2\, x_4}{(x_1 - x_3)(x_2 - x_3)(x_3 - x_4)}, \quad D = \frac{x_1\, x_2\, x_3}{(x_1 - x_4)(x_2 - x_4)(x_3 - x_4)}.$$

The formulae for higher-order BDFk ($k \geq 5$) with variable step sizes can also be derived similarly. We omit the detail here for brevity.

REFERENCES

[1] S.M. Allen and J.W. Cahn, *A microscopic theory for antiphase boundary motion and its application to antiphase domain coarsening*, Acta Metallurgica, 27 (1979), pp. 1085–1095.

[2] M.H. Anderson, J.R. Ensher, M.R. Matthews, C.E. Wieman, and E.A. Cornell, *Observation of Bose-Einstein condensation in a dilute atomic vapor*, Science, 269 (1995), pp. 198–201.

[3] W. Bao and Q. Du, *Computing the ground state solution of Bose–Einstein condensates by a normalized gradient flow*, SIAM J. Sci. Comput., 25 (2004), pp. 1674–1697.

[4] J.W. Barrett and J.F. Blowey, *Finite element approximation of a model for phase separation of a multi-component alloy with non-smooth free energy*, Numer. Math., 77 (1997), pp. 1–34.

[5] J.W. Barrett and J.F. Blowey, *Finite element approximation of a model for phase separation of a multi-component alloy with a concentration-dependent mobility matrix*, IMA J. Numer. Anal., 18 (1998), pp. 287–328.

[6] J.W. Cahn and J.E. Hilliard., *Free energy of a nonuniform system.* I. *Interfacial free energy*, J. Chem. Phys., 28 (1958), pp. 258–267.

[7] J.W. Cahn and J.E. Hilliard, *Free energy of a nonuniform system.* III. *Nucleation in a two-component incompressible fluid*, J. Chem. Phys., 31 (1959), pp. 688–699.

[8] E. Celledoni, V. Grimm, R.I. McLachlan, D.I. McLaren, D. O'Neale, B. Owren, and G.R.W. Quispel, *Preserving energy resp. dissipation in numerical PDEs using the "Average Vector Field" method*, J. Comput. Phys., 231 (2012), pp. 6770–6789.

[9] W. Chen, X. Wang, Y. Yan, and Z. Zhang, *A second order BDF numerical scheme with variable steps for the Cahn–Hilliard equation*, SIAM J. Numer. Anal., 57 (2019), pp. 495–525.

[10] Q. Cheng and J. Shen, *Multiple scalar auxiliary variable (MSAV) approach and its application to the phase-field vesicle membrane model*, SIAM J. Sci. Comput., 40 (2018), pp. A3982–A4006.

[11] Q. Cheng, J. Shen, and X.F. Yang, *Highly efficient and accurate numerical schemes for the epitaxial thin film growth models by using the SAV approach*, J. Sci. Comput., 78 (2019), pp. 1467–1487.

[12] C.M. Elliott and A.M. Stuart, *The global dynamics of discrete semilinear parabolic equations*, SIAM J. Numer. Anal., 30 (1993), pp. 1622–1663.

[13] D.J. Eyre, *Unconditionally gradient stable time marching the Cahn-Hilliard equation*, in Computational and Mathematical Models of Microstructural Evolution (San Francisco, CA, 1998), Warrendale, PA, 1998, pp. 39–46.

[14] F. Guillen-Gonzalez and G. Tierra, *On linear schemes for a Cahn-Hilliard diffuse interface model*, J. Comput. Phys., 234 (2013), pp. 140–171.

[15] Y. Gong, J. Zhao, and Q. Wang, *Arbitrarily high-order unconditionally energy stable schemes for thermodynamically consistent gradient flow models*, SIAM J. Sci. Comput., 42 (2020), pp. 135–156.

[16] Y. Gong, J. Zhao, and Q. Wang, *Arbitrarily high-order unconditionally energy stable SAV schemes for gradient flow models*, Comput. Phys. Commun., 249 (2020), pp. 107033.

[17] Y. He, Y. Liu, and T. Tang, *On large time-stepping methods for the Cahn-Hilliard equation*, Appl. Numer. Math., 57 (2006), pp. 616–628.

[18] X.L. Li and J. Shen, *Error Analysis of the SAV-MAC Scheme for the Navier-Stokes Equations*, e-print, arXiv:1909.05131, 2019.

[19] X.L. Li, J. Shen, and H.X. Rui, *Stability and error analysis of a second-order SAV scheme with block-centered finite differences for gradient flows*, Math. Comp., 88 (2019), pp. 2047–2068.

[20] L.L Lin, Z.G. Yang, and S.C. Dong, *Numerical approximation of incompressible Navier-Stokes equations based on an auxiliary energy variable*, J. Comput. Phys., 388 (2019), pp. 1–22.

[21] F. Lou, T. Tang, and H. Xie, *Parameter-free time adaptivity based on energy evolution for the Cahn-Hilliard equation*, Commun. Comput. Phys., 19 (2016), pp. 1542–1563.
[22] G.R.W. Quispel and D.I. McLaren, *A new class of energy-preserving numerical integration methods*, J. Phys. A, 41 (2008), 045206.
[23] J. Shen, J. Xu, and J. Yang, *The scalar auxiliary variable (SAV) approach for gradient flows*, J. Comput. Phys., 353 (2018), pp. 407–416.
[24] J. Shen, J. Xu, and J. Yang, *A new class of efficient and robust energy stable schemes*, SIAM Rev., 61 (2019), pp. 474–506.
[25] J. Shen, T. Tang, and L.L. Wang, *Spectral Methods: Algorithms, Analysis and Applications*, Springer, Berlin, 2011.
[26] J. Shen and X.F. Yang, *Numerical approximations of Allen-Cahn and Cahn-Hilliard equations*, Discrete Contin. Dyn. Syst., 28 (2010), pp. 1669–1691.
[27] X.F. Yang, *Linear, first and second-order, unconditionally energy stable numerical schemes for the phase field model of homopolymer blends*, J. Comput. Phys., 327 (2016), pp. 294–316.
[28] Z.G. Yang and S.C. Dong, *A roadmap for discretely energy-stable schemes for dissipative systems based on a generalized auxiliary variable with guaranteed positivity*, J. Comput. Phys., 404 (2020), 109121.
[29] Z.G. Yang and S.C. Dong, *An unconditionally energy-stable scheme based on an implicit auxiliary energy variable for incompressible two-phase flows with different densities involving only precomputable coefficient matrices*, J. Comput. Phys., 393 (2019), pp. 229–257.
[30] Z.G. Yang, L.L Lin, and S.C. Dong, *A family of second-order energy-stable schemes for Cahn-Hilliard type equations*, J. Comput. Phys., 383 (2019), pp. 24–54.
[31] Z. Zhang and Z. Qiao, *An adaptive time-stepping strategy for the Cahn-Hilliard equation*, Commun. Comput. Phys., 11 (2012), pp. 1261–1278.
[32] J. Zhao, Q. Wang, and X.F. Yang, *Numerical approximations for a phase field dendritic crystal growth model based on the invariant energy quadratization approach*, Internat. J. Numer. Methods Engrg., 110 (2017), pp. 279–300.
[33] J.Z. Zhu, L.Q. Chen, J. Shen, and V. Tikare, *Finite element approximation of a model for phase separation of a multi-component alloy with a concentration-dependent mobility matrix*, Phys. Rev. E, 60 (1999), pp. 35–64.
[34] Q.Q. Zhuang and J. Shen, *Efficient SAV approach for imaginary time gradient flows with applications to one-and multi-component Bose-Einstein condensates*, J. Comput. Phys., 396 (2019), pp. 72–88.